

An optimal prognostic model based on gene expression for clear cell renal cell carcinoma

DAN XU^{1,2*}, WANTAI DANG^{3*}, SHAOQING WANG², BO HU¹, LIANGHONG YIN¹ and BAOZHANG GUAN¹

¹Department of Nephrology, The First Affiliated Hospital of Jinan University, Guangzhou, Guangdong 510632; Departments of ²Nephrology and ³Rheumatology, The First Affiliated Hospital of Chengdu Medical College, Chengdu, Sichuan 610500, P.R. China

Received December 1, 2019; Accepted June 6, 2020

DOI: 10.3892/ol.2020.11780

Abstract. Clear cell renal cell carcinoma (ccRCC) is the most prevalent type of RCC; however, prognostic prediction tools for ccRCC are scant. Developing mRNA or long non-coding RNA (lncRNA)-based risk assessment tools may improve the prognosis in patients with ccRCC. RNA-sequencing and prognostic data from patients with ccRCC were downloaded from The Cancer Genome Atlas and the European Bioinformatics Institute Array database at the National Center for Biotechnology Information.

Differentially expressed (DE) RNAs (DERs) and prognostic DERs were screened between less favorable and favorable prognoses using the limma package in R 3.4.1, and analyzed using univariate and multivariate Cox regression analyses, respectively. Risk score models were constructed using optimal combinations of DEmRNAs and DElncRNAs identified using the Least Absolute Shrinkage And Selection Operator Cox regression model of the penalized package. Associations between risk score models and overall survival time were evaluated. Independent prognostic clinical factors were screened using univariate and multivariate Cox regression analyses, and nomogram models were constructed. Gene Ontology biological processes and Kyoto Encyclopedia of Genes and Genomes pathway enrichment analyses were conducted using the clusterProfiler package in R3.4.1. A total of 451 DERs were identified, including 404 mRNAs and 47 lncRNAs, between less favorable and favorable prognoses, and 269 DERs, including 233 mRNAs and 36 lncRNAs, were identified as independent prognostic factors. Optimal combinations including 10 DEmRNAs or 10 DElncRNAs were screened using four risk score models based on the status or expression levels of the 10 DEmRNAs or 10 DElncRNAs. The model based on the expression levels of the 10 DEmRNAs had the highest prognostic power. These prognostic DEmRNAs may be involved in biological processes associated with the inflammatory response, complement and coagulation cascades and neuroactive ligand-receptor interaction pathways. The present validated risk assessment tool based on the expression levels of these 10 DEmRNAs may help to identify patients with ccRCC at a high risk of mortality. These 10 DEmRNAs in optimal combinations may serve as prognostic biomarkers and help to elucidate the pathogenesis of ccRCC.

Correspondence to: Dr Lianghong Yin or Dr Baozhang Guan, Department of Nephrology, The First Affiliated Hospital of Jinan University, 601 West Huangpu Avenue, Guangzhou, Guangdong 510632, P.R. China
E-mail: ylhjinanuni@163.com
E-mail: guanbaozhang130@126.com

*Contributed equally

Abbreviations: AGR, anterior gradient homolog; AUC, area under the curve; ccRCC, clear cell renal cell carcinoma; COL18A1-AS1, collagen 18A1 antisense RNA 1; CSF, granulocyte-macrophage colony-stimulating factor; cvl, cross-validation likelihood; DE, differentially expressed; DEGs, DE genes; DER, DE RNA; EBI, European Bioinformatics Institute; ELOVL2-AS, elongation of very long-chain fatty acid 2-antisense RNA; FDR, false discovery rate; GAL3ST, galactose 3-O-sulfotransferase; GO, Gene Ontology; HGNC, Human Genome Organization Gene Nomenclature Committee; IGLL1, immunoglobulin λ -like polypeptide 1; KEGG, Kyoto Encyclopedia of Genes and Genomes; lncRNA, long non-coding RNA; LINC, long intergenic non-protein coding RNA; log2FC, log2-fold change; MIR205HG, microRNA 205 host gene; PLG, plasminogen; ROC, receiver operating characteristic; SAA, serum amyloid A; SOX, SRY-type HMG box transcription factor; SBSN, suprabasin; TCGA, The Cancer Genome Atlas; TCL, T cell leukemia/lymphoma; TFAP2A-AS1, transcription factor AP-2 α antisense RNA; UPK, uroplakin; WAP, whey acidic proteins; WFDC, WAP four-disulfide core domain protein; ZIC, zinc finger of the cerebellum

Key words: DEGs, lncRNAs, prognostic model, risk score, pathway enrichment analysis

Introduction

Clear cell renal cell carcinoma (ccRCC) accounts for 70-80% of all RCC and it is closely associated with von Hippel-Lindau tumor suppressor gene mutations (1,2). RCC comprises of a wide group of chemotherapy-resistant diseases that can be distinguished by histopathological features and underlying gene mutations (2); however, the variable biological behavior of early ccRCC usually leads to a failed diagnosis (3). The molecular pathogenesis of ccRCC also remains unclear. It is of

great clinical importance to fully understand the pathogenesis of ccRCC, at this would lead to the identification of reliable prognostic biomarkers and appropriate treatment selection.

The aberrant expression of coding genes and long non-coding RNAs (lncRNA) is usually associated with the emergence and development of various types of cancers, such as lung adenocarcinoma, ovarian cancer and ccRCC, and lncRNAs could serve as potential diagnostic markers (4-8). It is well known that ccRCC is associated with the following: Dysregulated oxidative phosphorylation, amino acid metabolism and oncogenic metabolism, such as the down-regulation of genes involved in the tricarboxylic acid cycle, decreased AMP-activated kinase and levels of PTEN protein, upregulation of the pentose phosphate pathway and glutamine transporter genes and increased acetyl-Coenzyme A carboxylase protein levels (2,9,10). lncRNAs are non-coding RNAs of >200 nucleotides in length, and numerous ccRCC-associated lncRNAs have been identified and applied as potential prognostic and diagnostic biomarkers, such as metastasis-associated lung adenocarcinoma transcript 1 and nuclear paraspeckle assembly transcript 1 (11-13). Despite considerable progress, the prognostic roles of coding genes and lncRNAs in ccRCC, and the underlying mechanisms remain poorly understood. Further functional investigation is required to explore more ccRCC-associated coding genes and lncRNAs, and to verify their functional mechanisms with respect to the prognosis in patients with ccRCC.

Disease progression is usually mediated by multiple relevant genes rather than by a single gene (14). It would be useful for both healthcare providers and patients to develop risk assessment tools that could detect populations at high risk of a disease and inform clinical decisions regarding treatment (15). Compared with the extensive application of risk assessment tools for various types of cancer, such as gastric cancer, hepatocellular carcinoma and prostate cancer (15-17), risk assessment tools for ccRCC remain scant. The disease-free survival of patients with localized ccRCC has mostly been predicted using an immunohistochemistry-based molecular signature of five markers, including Ki-67, p53, endothelial vascular endothelial growth factor receptor (VEGFR)-1, epithelial VEGFR-1, and epithelial vascular endothelial growth factor (VEGF)-D (18), and prognosis in patients with ccRCC has been assessed using expression-based mRNA and non-coding RNA signatures (11,19-21). Therefore, further risk assessment tools for ccRCC are required.

The present study analyzed large quantities of gene expression and corresponding clinical data of patients with ccRCC downloaded from The Cancer Genome Atlas (TCGA) and European Bioinformatics Institute (EBI) Array databases in the public domain. Differentially expressed RNAs (DERs) were identified and an optimal prognosis prediction model was constructed after comparing models based on the expression levels or status of prognostic DERs. The reliability of the prognostic prediction model was validated in two independent datasets. Furthermore, possible biological functions of the prognostic DERs in the pathogenesis of ccRCC were analyzed using Kyoto Encyclopedia of Genes and Genomes (KEGG) pathway enrichment analysis. The present study aimed to identify potential clinical diagnostic markers for ccRCC and to determine the possible pathogenesis of ccRCC.

Materials and methods

Data sources and preprocessing. The RNA expression profiles of ccRCC samples downloaded on April 5, 2019, from TCGA database (<https://gdc-portal.nci.nih.gov/>) were generated on an Illumina HiSeq 2000 RNA Sequencing platform. A total of 526 ccRCC tumor samples accompanied by relevant information about clinical survival were randomly assigned to either a training or validation set (n=263 in each). Table I shows the clinicopathological characteristics and prognostic information about the samples in the training, validation and training + validation (entire) sets. A gene expression dataset of patients with ccRCC (E-TABM-3267) (22), assessed on 22 January 2015 and last updated on 27 September 2018, was downloaded from the EBI Array database (<https://www.ebi.ac.uk/arrayexpress/>) (23) based on an Affymetrix GeneChip Human Gene 1.0 ST Array platform. The E-TABM-3267 dataset included 53 ccRCC tumor tissue samples with accompanying survival information, and served as an independent validation dataset.

Screening DERs in ccRCC samples

Annotation and identification of lncRNAs and mRNAs. According to probe location and ID provided in the downloaded annotation platform, lncRNAs and mRNAs in TCGA and EBI sets were annotated and identified from the Human Genome Organization Gene Nomenclature Committee (HGNC) database (<http://www.genenames.org/>), which comprises of 4,112 lncRNAs and 19,201 protein-encoding genes (24).

Screening of significant DERs. The 263 patients in the training set were classified as having a less favorable (overall survival time, <36 months) or a favorable (overall survival time, >60 months) prognosis. Significant DERs between the two prognostic groups in the training set were screened using the limma package (v3.34.7; <https://bioconductor.org/packages/release/bioc/html/limma.html>) (25) in R language (26) (v3.4.1). A false discovery rate (FDR) <0.05 and log 2-fold change (log₂FC) >0.5 were set as thresholds for determining significant DERs. Volcano plots of the DERs were created using the ggplot2 (27) package (v2.2.1) in R 3.4.1. Subsequently, pheatmap (v1.0.8; <https://cran.r-project.org/web/packages/pheatmap/index.html>) (28) in R 3.4.1 was used to analyze two-way hierarchical clustering of samples with a centered Pearson correlation algorithm based on DER expression.

Construction of prognostic model

Screening prognostic DERs. Based on the DERs screened in the aforementioned step, overall survival time in the training set was assessed via univariate and multivariate Cox regression analyses using a survival package (v2.41-1; <http://bioconductor.org/packages/survival/>) (29) in R 3.4.1 to identify DE mRNAs and DE lncRNAs with independent prognostic values, with log-rank P<0.05 as the cutoff of significance.

Screening optimal DER combinations. The Least Absolute Shrinkage And Selection Operator (LASSO) Cox regression model (30) of penalized package v0.9.50 (31)

Table I. Clinical information of the samples in the training (n=263), validation (n=263) and entire sets (n=526).

Clinical characteristics	Training set	Testing set	Entire set
Age, mean ± SD	60.84±11.73	60.24±12.52	60.54±12.12
Sex, male/female	171/92	171/92	342/184
Pathological M, M0/M1/-	213/35/15	207/42/14	420/77/29
Pathological N, N0/N1/-	118/8/137	120/8/135	238/16/272
Pathological T, T1/T2/T3/T4	141/31/87/4	128/38/90/7	269/69/177/11
Pathological stage, I/II/III/IV	137/26/61/39	126/31/62/44	263/57/123/83
Pathological grade, G1/G2/G3/G4/-	8/110/104/37/4	5/116/101/37/4	13/226/205/74/8
Platelet count elevated/low/normal/-	17/25/169/52	19/20/186/38	36/45/355/90
Serum calcium, elevated/low/normal/-	4/96/75/88	6/107/72/78	10/203/147/166
White cell count, elevated/low/normal/-	79/5/124/55	83/3/139/38	162/8/263/93
Death, dead/alive	86/177	86/177	172/354
Overall survival time, months ± SD	44.88±32.63	45.41±33.05	45.15±32.81

T, tumor; N, node; M, metastasis.

(<https://cran.r-project.org/web/packages/penalized/index.html>) in R 3.4.1 was used to uncover the optimal combinations of the aforementioned prognostic DE mRNAs and DE lncRNAs. The optimized parameter 'lambda' was generated via the cross-validation likelihood (cvl) of 1,000 measurements.

Diverse risk assessment models constructed based on optimal mRNAs or lncRNAs. Two categories of risk assessment models were constructed using multivariate Cox regression coefficients of the optimal combinations of DE mRNAs or DE lncRNAs.

Risk prediction models based on mRNA or lncRNA status. The cut-off values for amounts of optimal DE mRNA and DE lncRNA expression were calculated using the X-Tile Bio-Information Tool (32) (<https://medicine.yale.edu/lab/rimm/research/software.aspx>). The Monte-Carlo value $P < 0.05$ was set as the criterion to determine the optimal cut-off for RNA expression. The status of RNA expression in the samples was defined according to the cut-off for each RNA; RNA expression $>$ cut-off or $<$ cut-off was defined as status 1 or 0, respectively. Two risk assessment models of status risk score were established using a linear combination of expression status of the optimal mRNAs or lncRNAs, weighted by regression coefficients to calculate status risk scores for each sample according to the following formula: $\beta_{RNA_n} \times \text{Status}_{RNA_n}$, where β_{RNA_n} and Status_{RNA_n} represent the regression coefficient and status variable of RNA_n, respectively.

Risk prediction models based on expression levels of mRNAs or lncRNAs. Two risk prediction models of expression risk score were constructed based on the expression levels of optimal mRNA or lncRNA, and expression risk scores for all samples were calculated as follows: $\sum \beta_{RNA_n} \times \text{Expression}_{RNA_n}$, where β_{RNA_n} and $\text{Expression}_{RNA_n}$ represent the regression coefficient and the amount of RNA_n expression, respectively.

Evaluation and comparison of diverse risk prediction models. Samples in the training set were divided into high- and low-risk groups for each of the four prognosis prediction models, with the median risk score as the demarcation point. Associations between risk models and overall survival time were evaluated using Kaplan-Meier curves in the survival package (v2.41-1) in R 3.4.1. The sensitivity and specificity of risk scores to predict the overall survival time of patients were evaluated using receiver operating characteristic (ROC) curves. The predictive capability of these models was authenticated using the validation, entire and independent validation (E-TABM-3267) datasets. The optimal model was that with the greatest power to predict the prognosis in patients with ccRCC.

Establishment of a survival nomogram based on independent prognostic factors and the fittest risk score model

Screening independent prognostic clinical factors. Independent prognostic clinical factors were screened in samples in the training, validation and entire sets via univariate and multivariate Cox regression analysis using the survival package (v2.41-1) in R3.4.1. Log-rank values with $P < 0.05$ were chosen as thresholds for identifying significant prognostic clinical factors. Pathological stage of ccRCC was defined according to the 1997 TNM staging system (33). The tumors were graded following the Fuhrman nuclear grading system (34). Normal platelet count was defined as $100\text{-}300 \times 10^9/\text{l}$; elevated platelet count, $>300 \times 10^9/\text{l}$; low platelet count, $<300 \times 10^9/\text{l}$. Normal serum calcium levels are 2.25-2.75 mmol/l, elevated levels, >2.75 mmol/l and low levels <2.25 mmol/l. Normal white cell count was defined as $4.0\text{-}10.0 \times 10^9/\text{l}$, elevated count was $>10.0 \times 10^9/\text{l}$ and low count was $<4.0 \times 10^9/\text{l}$.

Construction of nomograms for 3- and 5-year survival probability. Associations between independent prognostic factors and prognosis were further analyzed as follows. Risk scores from the optimal prognostic prediction model were combined with the identified independent prognostic factors,

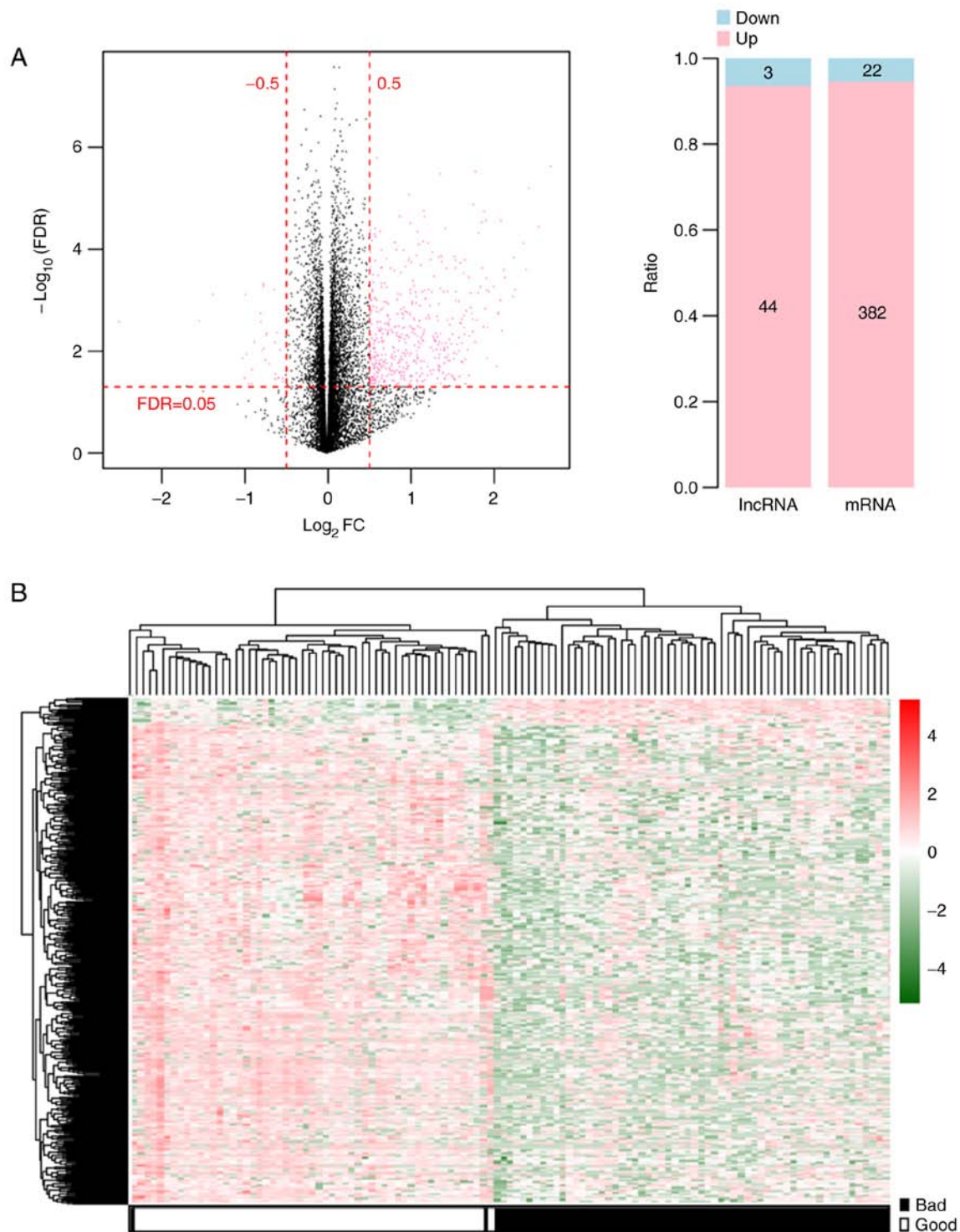


Figure 1. Identification and clustering of DEGs. (A) Left panel presents the volcano map of DEGs between less favorable and favorable prognoses. Pink dots represent DEGs. Black dots represent non-DEGs. Red horizontal and two vertical dashed lines represent $\text{FDR} < 0.05$ and $\log_2 \text{FC} > 0.5$, respectively. Right panel presents the composition of DEGs with the types and ratios on the horizontal and vertical axes, respectively. Blue and pink columns represent proportions of down- and upregulated RNAs, respectively. (B) Two-way hierarchical clustering heatmap based on the expression levels of DEGs. The black and white bars represent less favorable and favorable prognostic groups, respectively. The color key (green to red) exhibits z-score of normalized and \log_2 transformed expression values of DEGs. The Z-score represents the number of median absolute deviation away from the median. DEGs, differentially expressed RNAs; lncRNA, long non-coding RNA; FDR, false discovery rate; FC, fold change.

and nomograms were constructed for 3- and 5-year survival probability using the rms package (v5.1-2) (35,36) in R 3.4.1 (<https://cran.r-project.org/web/packages/rms/index.html>). Nomograms enable the visualization of regression equations. Scoring criteria are formulated by the magnitude of the

regression coefficients of all independent variables. Scales of each independent variable are scored, and a total score can be estimated for each sample. The probability and outcome for each sample can then be calculated using a conversion function between the score and the probability that the outcome

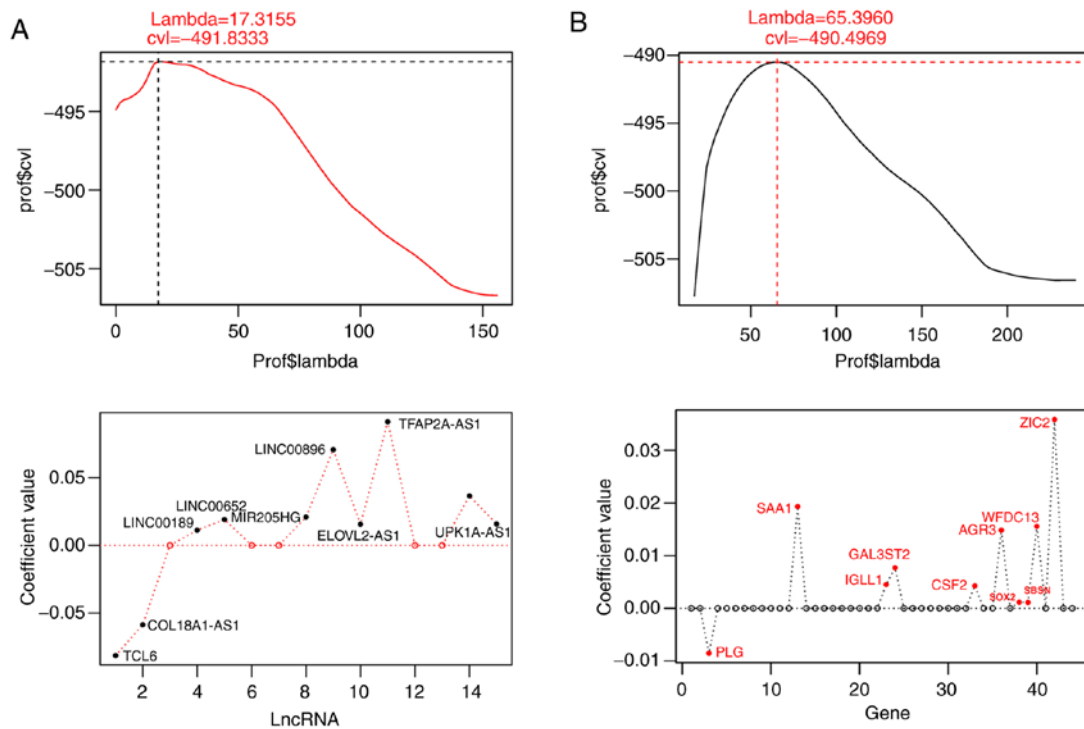


Figure 2. Screening curves of lambda parameters and distribution graphs of coefficients of the optimal combination of (A) lncRNAs and (B) mRNAs via the Cox-PH model based on the L1-penalized regularized regression algorithm. Horizontal and vertical axes in upper graphs indicate lambda and cvl values, respectively. prof stands for profL1 function, and \$ indicates the absolute reference. Intersection of red dotted lines indicate the value of lambda when cvl is maximal. When maximal cvl values were -491.8333 and -490.4969, lambda values were 17.3155 for mRNA and 65.3960 for lncRNA, respectively. lncRNA, long non-coding RNA; cvl, cross-validation likelihood.

will occur (37). Probabilities derived from nomograms were used to evaluate and predict associations between independent prognostic factors and the prognosis of targets.

Functional analysis of DE genes (DEGs) in high-and low-risk groups in the entire set. Samples in the entire set were divided into high- and low-risk groups according to risk scores obtained from the fittest prognostic prediction model. Differences in the expression matrix of genes between the high- and low-risk groups were investigated using the limma package (v3.34.7) in R 3.4.1. FDR <0.05 and $\log_2FC >0.263$ were set as the threshold for identifying DEGs, and a volcano plot of significant DEGs was created using the ggplot2 package in R 3.4.1. Gene Ontology (GO) of biological processes and KEGG pathway enrichment analysis of the identified DEGs were performed using the clusterProfiler package (v3.6.0) in R 3.4.1 language (38) ([http:// bioconductor.org/packages/release/bioc/html/clusterProfiler.html](http://bioconductor.org/packages/release/bioc/html/clusterProfiler.html)). $P <0.05$ was considered to indicate a statistically significant difference.

Results

Identification of DERs

Annotation of lncRNAs and mRNAs. According to probe location provided in the downloaded platforms, 19,021 mRNAs and 376 lncRNAs were annotated in TCGA set, and 18,007 mRNAs and 402 lncRNAs were annotated in E-TABM-3267 using the HGNC database. After removing the mRNAs and lncRNAs with a value of 0 in all samples, the two datasets

had 17,097 mRNAs and 376 lncRNAs in common (data not shown).

Screening DERs. The RNA expression profiles of 526 ccRCC tumor samples were downloaded from TCGA database with corresponding clinical data. These samples were randomly and equally divided into training (n=263) and testing (n=263) sets. Among the 263 ccRCC cancer samples in the training set, the prognosis of 53 samples was defined as less favorable and that of 63 samples was defined as favorable. A total of 451 significant DERs with FDR <0.05 and $\log_2FC >0.5$ were identified between the two prognoses groups from the volcano plot generated using the limma package (Fig. 1A). These DERs comprised 404 (22 downregulated and 382 upregulated) mRNAs and 47 (three downregulated and 44 upregulated) lncRNAs (Fig. 1A). Two-way hierarchical clustering heatmaps showed that the samples clustered into two groups (Fig. 1B).

Construction of prognostic models

Screening independent prognostic DER. Univariate Cox regression analysis was used to screen 269 prognostic DERs, including 233 mRNAs and 36 lncRNAs from the 451 DERs identified according to the overall survival time of patients in the aforementioned step. Multivariate Cox regression analysis then selected 44 mRNAs and 15 lncRNAs as independent prognostic factors (data not shown).

Screening optimal DER combinations. Using the expression values of the identified 44 mRNAs and 15 lncRNAs of independent prognostic values as input, the combination of

Table II. Detailed information of the optimal combinations of 10 DElncRNAs or 10 DEmRNAs.

RNA	Coefficient	P-value	HR	95% CI	Cut-off
mRNA					
AGR3	0.0148287	9.65x10 ⁻³	1.2059	1.0465-1.3895	-0.13
CSF2	0.0042776	9.22x10 ⁻⁵	1.4426	1.2005-1.7334	0.40
GAL3ST2	0.0076842	1.69x10 ⁻²	1.3308	1.0527-1.6822	0.51
IgLL1	0.0045121	2.50x10 ⁻³	1.2333	1.0765-1.4130	0.41
PLG	-0.008533	1.88x10 ⁻³	0.7408	0.6131-0.8951	-0.67
SAA1	0.0193154	1.28x10 ⁻⁴	1.8849	1.3629-2.6068	0.62
SBSN	0.0155634	9.34x10 ⁻³	1.2852	1.0636-1.5528	0.55
SOX2	0.0011085	2.76x10 ⁻⁴	1.3625	1.1533-1.6097	0.28
WFDC13	0.0011551	2.06x10 ⁻⁴	1.3922	1.1690-1.6581	0.65
ZIC2	0.0358394	1.43x10 ⁻²	1.2846	1.0512-1.5698	0.42
lncRNA					
COL18A1-AS1	-0.058594	2.02x10 ⁻³	0.8678	0.7790-0.9668	0.07
ELOVL2-AS1	0.0155223	2.75x10 ⁻²	1.0463	1.0056-1.1106	-0.06
LINC00189	0.0112113	1.61x10 ⁻²	1.0769	1.0011-1.1701	-0.02
LINC00470	0.036526	3.48x10 ⁻²	1.0574	1.0056-1.1461	-0.23
LINC00652	0.0190087	4.50x10 ⁻²	1.1313	1.0927-1.3806	0.07
LINC00896	0.0707072	2.65x10 ⁻²	1.0775	1.0060-1.1875	0.83
MIR205HG	0.0209242	4.94x10 ⁻²	1.0344	1.0019-1.0952	0.04
TCL6	-0.081477	1.39x10 ⁻²	0.9224	0.8453-0.9964	-0.13
TFAP2A-AS1	0.0910578	9.28x10 ⁻³	1.1224	1.0019-1.2574	0.46
UPK1A-AS1	0.015775	1.66x10 ⁻²	1.0481	1.0039-1.1053	0.20

DElncRNA, differentially expressed long non-coding RNA; HR, hazard ratio; AGR3, anterior gradient 3; CSF2, colony stimulating factor 2; GAL3ST2, galactose-3-O-sulfotransferase 2; IgLL1, immunoglobulin lambda like polypeptide 1; PLG, plasminogen; SAA1, serum amyloid A1; SBSN, suprabasin; SOX2, SRY-box transcription factor 2; WFDC13, WAP four-disulfide core domain 13; ZIC2, Zic family member 2; COL18A1-AS1, collagen antisense RNA 1; ELOVL2-AS1, elongation of very long-chain fatty acid 2 antisense RNA 1; LINC, long intergenic non-protein coding RNA; MIR205HG, microRNA 205 host gene; TCL6, T cell leukemia/lymphoma 6; TFAP2A-AS1, transcription factor AP-2 alpha antisense RNA 1; UPK1A-AS1, uroplakin 1A antisense RNA 1.

predictive mRNAs or lncRNAs was further optimized and identified using the Cox regression model based on LASSO regularization regression algorithm in the penalized package. When the maximum value of cvl was -491.8333, the lambda value was 17.3155, obtaining an optimal combination of 10 mRNAs comprising anterior gradient homolog 3 (AGR3), granulocyte-macrophage colony-stimulating factor (CSF2), galactose 3-O-sulfotransferase (GAL3ST2), immunoglobulin λ -like polypeptide 1 (IgLL1), plasminogen (PLG), serum amyloid A1 (SAA1), suprabasin (SBSN), SRY-type HMG box transcription factor 2 (SOX2), whey acidic protein (WAP) four-disulfide core domain protein (WFDC13) and zinc finger of the cerebellum family member 2 (ZIC2) (Fig. 2A). When the cvl reached the maximum value of -490.4969, lambda was 65.3960, and an optimal combination of 10 significant lncRNAs was retrieved, comprising of collagen 18A1 antisense RNA 1 (COL18A1-AS1), elongation of very long-chain fatty acid 2 antisense RNA 1 (ELOVL2-AS1), long intergenic non-protein coding RNA 189 (LINC00189), LINC00470, LINC00652, LINC00896, microRNA 205 host gene (MIR205HG), T cell leukemia/lymphoma 6 (TCL6), transcription factor AP-2 α antisense RNA (TFAP2A-AS1) and uroplakin 1A antisense RNA 1 (UPK1A-AS1) (Fig. 2B). Regression coefficients,

P-values, hazard ratios (HRs) and 95% CIs of the 10 significant lncRNAs and 10 significant mRNAs derived from the LASSO Cox regression model are listed in Table II. P-values of all the 10 lncRNAs and 10 mRNAs were all <0.05.

Construction of risk prediction models based on optimal combinations of 10 mRNAs or 10 lncRNAs. Various types of risk prediction models were constructed based on the regression coefficients of the optimal combinations of the aforementioned 10 prognostic mRNAs or lncRNAs (Table II).

Risk prediction models based on mRNA expression status (I). Associations between expression levels of the identified combinations of 10 DElncRNAs or 10 DEmRNAs in samples and overall survival time were analyzed in the training set using the X-Tile Bio-Informatics Tool. Table II shows the cut-off values for the expression levels of each DElncRNA or DEmRNA.

According to the cut-off value of each RNA, the status of samples with lower and higher expression was set to 0 and 1, respectively. Consequently, the following prediction model based on the status of 10 mRNAs or 10 lncRNAs was constructed: mRNA Status risk score = 0.0148287 x Status_{AGR3}

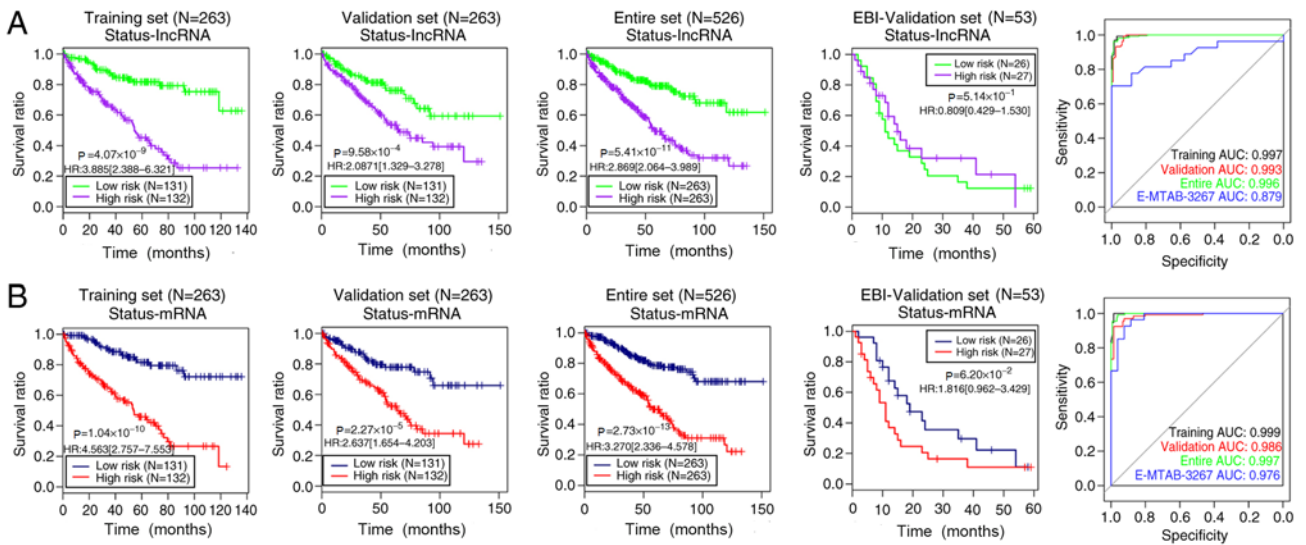


Figure 3. Kaplan-Meier overall survival time and ROC curves of risk score models based on the status of (A) 10 lncRNAs and (B) 10 mRNAs in the training, validation, entire and EBI-validation sets. Green/blue and red/purple curves represent low and high risk groups, respectively. In the ROC curves, the black, red, green and blue lines indicate the training, validation, entire and EBI-validation sets, respectively. lncRNA, long non-coding RNA; EBI, European Bioinformatics Institute; ROC, receiver operating characteristic; AUC, area under the curve; HR, hazard ratio.

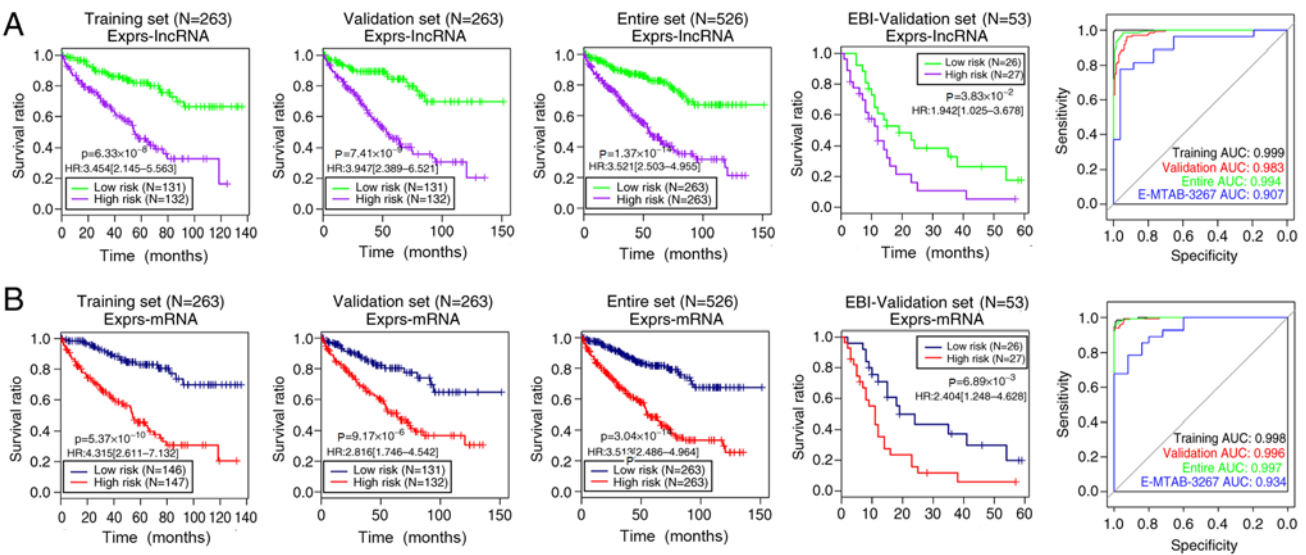


Figure 4. Kaplan-Meier curves for overall survival time and ROC analysis of risk score models based on the expression levels of (A) 10 lncRNAs and (B) 10 mRNAs in the training, validation, entire and EBI-validation sets. Green/blue and red/purple curves represent the low and high risk groups, respectively. In the ROC curves, the black, red, green and blue lines indicate the training, validation, entire and EBI-validation sets, respectively. lncRNA, long non-coding RNA; EBI, European Bioinformatics Institute; ROC, receiver operating characteristic; AUC, area under the curve; HR, hazard ratio; Exprs, expression levels.

$$\begin{aligned}
 &+ (0.0042776) \times \text{Status}_{\text{CSF2}} + (0.0076842) \times \text{Status}_{\text{GAL3ST2}} + \\
 &(0.0045121) \times \text{Status}_{\text{IGLL1}} + (-0.008533) \times \text{Status}_{\text{PLG}} + \\
 &(0.0193154) \times \text{Status}_{\text{SAA1}} + (0.0155634) \times \text{Status}_{\text{SBSN}} + \\
 &(0.0011085) \times \text{Status}_{\text{SOX2}} + (0.0011551) \times \text{Status}_{\text{WFDC13}} + \\
 &(0.0358394) \times \text{Status}_{\text{ZIC2}}; \text{ lncRNA Status risk score} = \\
 &-0.058594 \times \text{Status}_{\text{COL18A1-AS1}} + (0.0155223) \times \text{Status}_{\text{ELOVL2-AS1}} \\
 &+ (0.0112113) \times \text{Status}_{\text{LINC00189}} + (0.036526) \times \text{Status}_{\text{LINC00470}} + \\
 &(0.0190087) \times \text{Status}_{\text{LINC00652}} + (0.0707072) \times \text{Status}_{\text{LINC00896}} \\
 &+ (0.0209242) \times \text{Status}_{\text{MIR205HG}} + (-0.081477) \times \text{Status}_{\text{TCL6}} + \\
 &(0.0910578) \times \text{Status}_{\text{TFAP2A-AS1}} + (0.015775) \times \text{Status}_{\text{UPK1A-AS1}}.
 \end{aligned}$$

Risk prediction models based on expression levels (II). The following prediction models were created based on expression

levels (Exprs) of the mRNAs or lncRNAs in the aforementioned step: mRNA Expression risk score = 0.0148287 x ExprsAGR3 + (0.0042776) x ExprsCSF2 + (0.0076842) x ExprsGAL3ST2 + (0.0045121) x ExprsIGLL1 + (-0.008533) x ExprsPLG + (0.0193154) x ExprsSAA1 + (0.0155634) x ExprsSBSN + (0.0011085) x ExprsSOX2 + (0.0011551) x ExprsWFDC13 + (0.0358394) x ExprsZIC2; lncRNA Expression risk score = -0.058594 x ExprsCOL18A1-AS1 + (0.0155223) x ExprsELOVL2-AS1 + (0.0112113) x ExprsLINC00189 + (0.036526) x ExprsLINC00470 + (0.0190087) x ExprsLINC00652 + (0.0707072) x ExprsLINC00896 + (0.0209242) x ExprsMIR205HG + (-0.081477) x ExprsTCL6 + (0.0910578) x ExprsTFAP2A-AS1 + (0.015775) x ExprsPK1A-AS1.

Table III. Independent prognostic clinical factors identified by univariate and multivariate Cox regression analysis.

A, Training set (n=263)				
Clinical characteristics	Univariate analysis		Multivariate analysis	
	HR (95% CI)	P-value	HR (95% CI)	P-value
Age, <60/≥60 years	1.028 (1.009-1.047)	3.12x10 ⁻³	1.026 (1.0032-1.049)	2.48x10 ⁻²
Sex, male/female	1.186 (0.755-1.862)	4.59x10 ⁻¹	-	-
Pathological M, M0/M1/-	4.396 (0.782-6.945)	4.25x10 ⁻¹	-	-
Pathological N, N0/N1/-	3.007 (0.779-7.670)	1.55x10 ⁻¹	-	-
Pathological T, T1/T2/T3/T4	2.170 (1.701-2.767)	1.71x10 ⁻¹¹	1.761 (0.952- 2.279)	3.02x10 ⁻¹
Pathological stage, I/II/III/IV/-	1.995 (1.657-2.403)	2.44x10 ⁻¹⁵	1.759 (1.179-2.627)	5.69x10 ⁻³
Neoplasm histologic grade, G1/G2/G3/G4/-	2.536 (1.893-3.397)	1.28x10 ⁻¹⁰	1.361 (0.952-1.945)	9.07x10 ⁻²
Platelet count, elevated/low/normal/-	0.629 (0.517-0.765)	1.10x10 ⁻⁶	0.832 (0.679-1.017)	7.30x10 ⁻²
Serum calcium, elevated/low/normal/-	1.179 (0.738-1.884)	4.90x10 ⁻¹	-	-
White cell count, elevated/low/normal/-	1.159 (0.899-1.496)	2.54x10 ⁻¹	-	-
mRNA expression model				
Risk score status, high/low	4.315 (2.611-7.132)	5.37x10 ⁻¹⁰	2.626 (1.426-4.838)	1.95x10 ⁻³
B, Validation set (n=263)				
Clinical characteristics	Univariate analysis		Multivariate analysis	
	HR (95% CI)	P-value	HR (95% CI)	P-value
Age, <60/≥60 years	1.028 (1.011-1.046)	1.41x10 ⁻³	1.034 (1.013-1.055)	1.35x10 ⁻³
Sex, male/female	0.755 (0.491-1.162)	2.00x10 ⁻¹	-	-
Pathological M, M0/M1/-	4.189 (2.710-6.475)	5.41x10 ⁻²	-	-
Pathological N, N0/N1/-	3.947 (1.649-9.450)	8.72x10 ⁻²	-	-
Pathological T, T1/T2/T3/T4	1.725 (1.375-2.164)	1.1-x10 ⁻⁶	0.716 (0.474-1.082)	1.13x10 ⁻¹
Pathological stage, I/II/III/IV/-	1.786 (1.481-2.154)	1.31x10 ⁻¹⁰	2.006 (1.424-2.825)	6.84x10 ⁻⁵
Neoplasm histologic grade, G1/G2/G3/G4/-	2.075 (1.557-2.765)	3.37x10 ⁻⁷	1.245 (0.906-1.712)	1.76x10 ⁻¹
Platelet qualitative, elevated/low/normal/-	0.602 (0.453-0.8001)	3.07x10 ⁻⁴	0.749 (0.560-1.001)	5.04x10 ⁻²
Serum calcium, elevated/low/normal/-	0.752 (0.477-1.186)	2.20x10 ⁻¹	-	-
White cell count, elevated/low/normal/-	1.116 (0.879-1.416)	3.68x10 ⁻¹	-	-
mRNA expression model				
Risk score status, high/low	2.816 (1.746-4.542)	9.17x10 ⁻⁶	1.986 (1.168-.379)	1.14x10 ⁻²
C, Entire set (n=526)				
Clinical characteristics	Univariate analysis		Multivariate analysis	
	HR (95% CI)	P-value	HR (95% CI)	P-value
Age, <60/≥60 years	1.028 (1.015-1.041)	1.25x10 ⁻⁵	1.022 (1.001-1.0429)	3.59x10 ⁻²
Sex, male/female	0.943 (0.692-1.287)	7.13x10 ⁻¹	-	-
Pathological M, M0/M1/-	4.270 (0.919-5.845)	6.32x10 ⁻²	-	-
Pathological N, N0/N1/-	3.461 (1.836-6.526)	4.38x10 ⁻⁵	1.007 (0.429-2.361)	9.87x10 ⁻¹
Pathological T, T1/T2/T3/T4	1.914 (1.624-2.255)	4.44x10 ⁻¹⁶	0.703 (0.451-1.098)	1.22x10 ⁻¹
Pathological stage, I/II/III/IV/-	1.884 (1.652-2.15)	2.00x10 ⁻¹⁶	1.815 (1.278-2.577)	8.68x10 ⁻⁴
Neoplasm histological grade, G1/G2/G3/G4/-	2.285 (1.863-2.802)	3.33x10 ⁻¹⁶	1.359 (0.9591.926)	8.39x10 ⁻²
Platelet qualitative, elevated/low/normal/-	0.648 (0.552-0.763)	1.02x10 ⁻⁷	0.746 (0.594-0.936)	1.12x10 ⁻²
Serum calcium levels, elevated/low/normal/-	0.938 (0.677-1.298)	6.98x10 ⁻¹	-	-
White cell count, elevated/low/normal/-	1.135 (0.954-1.351)	1.53x10 ⁻¹	-	-

Table III. Continued.

Clinical characteristics	Univariate analysis		Multivariate analysis	
	HR (95% CI)	P-value	HR (95% CI)	P-value
mRNA expression model				
Risk score status, high/low	3.513 (2.486-4.964)	3.04×10^{-14}	2.943 (1.666-5.200)	2.02×10^{-4}

HR, hazard ratio; T, tumor; N, node; M, metastasis.

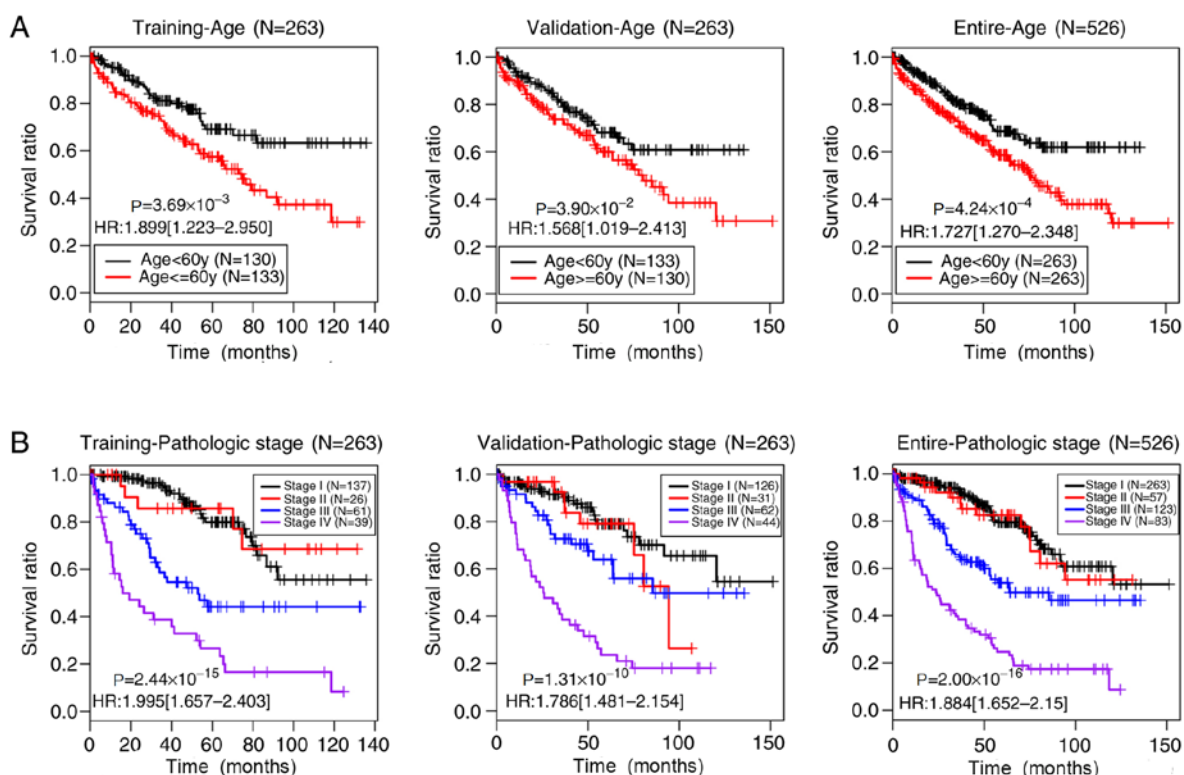


Figure 5. Kaplan-Meier overall survival curves for training (left), validation (middle) and entire (right) sets by (A) age and (B) pathologic stage. (A) Black and red curves indicate <60 and ≥ 60 years, respectively. (B) Black, red, blue and purple curves represent stages I, II, III and IV, respectively. HR, hazard ratio.

Effectiveness evaluation and comparison of prognosis prediction models. The predictive abilities of the four models were evaluated and compared among the training, validation, entire and E-MTAB-3267 (independent validation) sets (Figs. 3 and 4). The training [lncRNAs-based status risk score: log-rank $P=4.07 \times 10^{-9}$; HR (95% CI), 3.885 (2.388-6.321); mRNAs-based status risk score: log-rank $P=1.04 \times 10^{-10}$; HR (95% CI), 4.653 (2.757-7.553)], validation [lncRNAs-based status risk score: log-rank $P=9.58 \times 10^{-4}$; HR (95% CI), 2.087 (1.329-3.278); mRNAs-based status risk score: log-rank $P=2.27 \times 10^{-5}$; HR (95% CI), 2.637 (1.654-4.203)] and entire [lncRNAs-based status risk score: log-rank $P=5.41 \times 10^{-11}$; HR (95% CI), 2.869 (2.064-3.989); mRNAs-based status risk score: log-rank $P=2.73 \times 10^{-13}$; HR (95% CI), 3.270 (2.336-4.578)] sets were separated into a high-risk group (shorter overall survival time) and a low-risk group (longer

overall survival time) using the status model based on the 10 lncRNAs or 10 mRNAs, respectively (Fig. 3). However, the two status models could not dichotomize the E-MTAB-3267 set into two risk groups with significantly different overall survival time (log-rank $P=5.14 \times 10^{-1}$ for lncRNA and 6.20×10^{-2} for mRNA; Fig. 3; Table III). Furthermore, all four datasets exhibited significantly different overall survival time between the high- and low-risk groups determined using the 10 lncRNA expression model (Fig. 4A): training set, log-rank $P=6.33 \times 10^{-8}$; HR (95% CI), 3.454 (2.145-5.563); validation set, log-rank $P=7.41 \times 10^{-9}$; HR (95% CI), 3.947 (2.389-6.521); entire set, log-rank $P=1.37 \times 10^{-14}$; HR (95% CI), 3.521 (2.503-4.955); E-MTAB-3267, log-rank $P=3.83 \times 10^{-2}$; HR (95% CI), 1.942 (1.025-3.678). Similar results were obtained using the 10 mRNA expression model (Fig. 4B): training set, log-rank $P=5.37 \times 10^{-10}$; HR (95% CI), 4.315 (2.611-7.132);

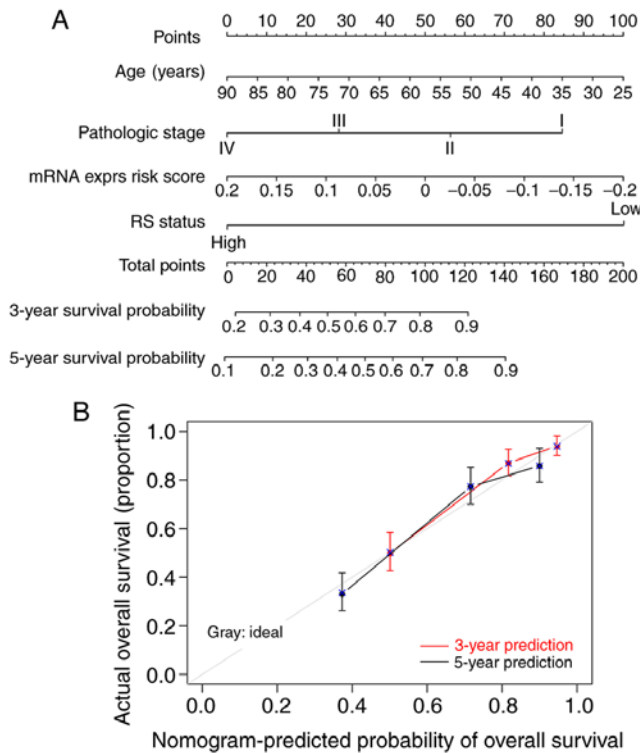


Figure 6. Nomogram of independent prognostic factors and mRNA expression risk scores, and calibration plots for predicting 3- and 5-year survival probabilities. (A) Nomogram of independent prognostic factors and mRNA expression risk scores. Points for each variable (age, pathological stage and mRNA expression risk score) were determined in the nomogram by drawing a vertical line from the values of each variable to the 'points' line. Summed points for all variables were plotted on the 'Total Points' line and a vertical line was drawn to read the corresponding 3- and 5-year survival probabilities. (B) Calibration plots for predicting 3- and 5-year survival probabilities. Horizontal and vertical axes indicate predicted and actual 3- and 5-year probabilities of overall survival time, respectively. Red and black lines indicate predicted 3- and 5-year probabilities of overall survival time, respectively. Round points on lines represent the average survival probability at corresponding time points with upper and lower bars indicating upper and lower standard deviations. Grey line represents ideal agreement between predicted and actual probabilities of overall survival time. exprs, expression; RS status, risk score status.

validation set, log-rank $P=9.17 \times 10^{-6}$; HR (95% CI), 2.816 (1.746-4.542); entire set, log-rank $P=3.04 \times 10^{-14}$; HR (95% CI), 3.513 (2.486-4.964); E-MTAB-3267, log-rank $P=6.89 \times 10^{-3}$; HR (95% CI), 2.404 (1.248-4.628). Additionally, Figs. 3 and 4 show the ROC curves and areas under the ROC curves (AUC) of the four models for the training, validation, entire and E-MTAB-3267 sets. The aforementioned results suggested that the risk assessment model based on the expression levels of the 10 mRNAs yielded more significant or similar log-rank P -values, and higher or similar AUC values compared with the other three models in the four datasets. Therefore, this model was selected as the best prognostic model and was applied in further analyses.

Establishment of nomogram survival model with independent prognostic clinical factors and 10 DE mRNA expression risk scores. Independent clinical prognostic factors for ccRCC were analyzed using univariate and multivariate Cox regression analyses of the samples. Table III shows that age,

pathological stage and mRNA expression model risk score status were identified as independent prognostic factors in the training, validation and entire sets ($P < 0.05$). Fig. 5 shows the Kaplan-Meier curves of age and pathological stage in these three sets. The prognoses of younger patients (< 60 years) and of patients at earlier pathological stages of ccRCC were significantly improved compared with those of older patients (≥ 60 years) (training set, $P=3.69 \times 10^{-3}$; validation set, $P=3.90 \times 10^{-2}$; entire set, $P=4.24 \times 10^{-4}$) and of patients with later pathological stages (training set, $P=2.44 \times 10^{-15}$; validation set, $P=1.31 \times 10^{-10}$; entire set, $P=2.00 \times 10^{-16}$), respectively, which was consistent with current clinical practice (39).

Establishment of nomogram survival model integrating 10 mRNA expression risk scores with independent prognostic factors. A composite nomogram was constructed using the entire set to further assess associations between prognosis and age, pathological stage and mRNA expression. Fig. 6A shows the nomogram of combined age, pathological stage and mRNA expression model risk score status to predict the survival of patients with ccRCC as the 'total points' axis of the sixth row. Total points represent the total account of points of age, pathological stage and mRNA expression model risk score. Calibration curves revealed good consistency between the 3- and 5-year survival probabilities of all patients of the entire set and those predicted by the nomogram survival model (Fig. 6B).

Identification and pathway enrichment analysis of DEG in high- and low-risk groups of entire set. The present study aimed to resolve the possible functional roles of the 10 prognostic mRNAs in ccRCC. Samples in the entire set were divided into high- and low-risk groups by applying the optimal risk score prediction model dependent on the expression levels of the 10 DE mRNAs. A total of 400 significant DEGs (including 19 downregulated and 381 upregulated genes) with $FDR < 0.05$ and $\log_2 FC > 0.263$ were identified using the limma package (Fig. 7A). An expression heatmap of the DEGs revealed distinctive expression patterns of DEGs with high and low risk scores (Fig. 7B). Subsequently, enrichment analyses of GO biological processes and KEGG signaling pathways for these DEGs were conducted. The results revealed that 11 biological processes, such as 'inflammatory response', 'neuron differentiation' and 'acute inflammatory response', and six KEGG signaling pathways, including 'complement and coagulation cascades' and 'neuroactive ligand-receptor interactions', were significantly enriched within these DEGs (Table IV).

Discussion

Considering that aberrant expression levels of mRNAs and lncRNAs are usually associated with the occurrence and development of ccRCC (2,9-13,20), exploring further lncRNA/mRNA-based signatures to predict the prognosis in patients with ccRCC should be important. In the present study, a large quantity of RNA-sequencing and survival data of patients with ccRCC was downloaded, and DEGs were screened between samples of patients with less favorable and favorable prognoses using models that could predict prognosis. Among

Table IV. GO biological processes and KEGG pathways significantly enriched by the differentially expressed genes.

Term	Count	P-value
Biological processes		
GO:0006953 acute-phase response	11	5.25x10 ⁻⁹
GO:0007586 digestion	13	3.08x10 ⁻⁷
GO:0002526 acute inflammatory response	13	6.99x10 ⁻⁷
GO:0030182 neuron differentiation	27	1.08x10 ⁻⁶
GO:0035270 endocrine system development	10	1.04x10 ⁻⁵
GO:0051606 detection of stimulus	11	1.49x10 ⁻⁴
GO:0007398 ectoderm development	14	2.25x10 ⁻⁴
GO:0030900 forebrain development	12	2.85x10 ⁻⁴
GO:0006954 inflammatory response	18	3.73x10 ⁻⁴
GO:0032101 regulation of response to external stimulus	12	4.19x10 ⁻⁴
GO:0009611 response to wounding	24	5.40x10 ⁻⁴
KEGG pathways		
hsa04080: Neuroactive ligand-receptor interaction	17	1.07x10 ⁻⁵
hsa00590: Arachidonic acid metabolism	5	1.80x10 ⁻²
hsa00591: Linoleic acid metabolism	4	1.35x10 ⁻²
hsa04060: Cytokine-cytokine receptor interaction	10	4.62x10 ⁻²
hsa00592: alpha-Linolenic acid metabolism	3	4.11x10 ⁻²
hsa04610: Complement and coagulation cascades	5	3.55x10 ⁻²

'Count' represents the number of genes significantly enriched in a biological process or pathway. GO, Gene Ontology; KEGG, Kyoto Encyclopedia of Genes and Genomes.

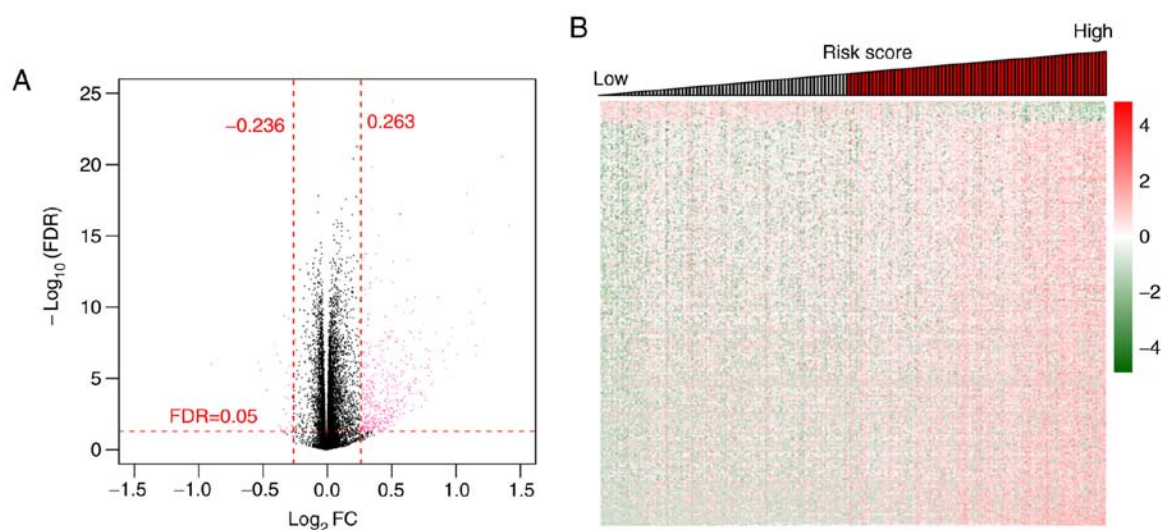


Figure 7. Volcano plot and expression heatmap of DEGs between high and low risk in the entire set. (A) Volcano plot of log2FC vs. $-\log_{10}$ FDR. Pink and black dots represent significant and non-significant DEGs, respectively. Two vertical dashed lines indicate log2FC 0.263; horizontal dashed line indicates FDR = 0.05. (B) Expression heatmap of DEGs with high or low risk scores. Colored bar (green to red) on right margin indicates z-score of normalized and log2 transformed expression values of DEGs. The Z-score represents for the number of median absolute deviations away from the median. DEG, differentially expressed genes; FDR, false discovery rate; FC, fold change.

the 451 DEs obtained from the training set, 404 and 47 were mRNAs and lncRNAs, respectively. Univariate and multivariate Cox regression analyses selected 44 mRNAs and 15 lncRNAs as independent prognostic factors. Furthermore, optimal combinations of 10 DE mRNAs (AGR3, CSF2, GAL3ST2, IGLL1, PLG, SAA1, SBSN, SOX2, WFDC13 and ZIC2) and

10 DE lncRNAs (COL18A1-AS1, ELOVL2-AS1, LINC00189, LINC00470, LINC00652, LINC00896, MIR205HG, TCL6, TFAP2A-AS1 and UPK1A-AS1) were screened out based on the findings of the LASSO Cox regression model.

Given the important roles of risk assessment tools in estimating the probability of risk factors and detecting

high-risk populations for disease entities (14-17), the present study constructed four prognostic prediction models based on the status or expression levels of the 10 DElncRNAs or 10 DErnRNAs in optimal combinations. The predictive value of the four models for ccRCC was assessed, and the results revealed that the risk score model based on the expression levels of the 10 DErnRNAs was the best predictor. Although risk assessment tools have been widely applied to the clinical prediction of various types of cancer, such as gastric cancer, hepatocellular carcinoma and prostate cancer, few are available for ccRCC (11,18-21). The present study created a potential risk assessment tool with which to predict the prognosis in patients with ccRCC, and to explore the possible pathogenesis of ccRCC.

According to the association with different types of cancer, especially ccRCC, the 10 DErnRNAs in the optimal combination can be divided into three groups. *AGR3*, *CSF2*, *GAL3ST2*, *SAA1*, *SBSN*, *SOX2* and *ZIC2* in the first group are all associated with human tumors. *AGR3* was originally identified as a membrane protein from breast cancer cell lines, and it has been implicated in the growth, differentiation, metastasis and survival of breast, prostate and ovarian cancer (40-43). *CSF2* is an important survival, proliferation and differentiation factor of neutrophil and macrophage progenitors (44). *CSF2* overexpression is associated with a poor prognosis in patients with urothelial carcinoma, suggesting that *CSF2* may serve as an important prognosticator and a potential therapeutic target for urothelial carcinoma (45). *GAL3ST2* functions in regulating adhesion capacity and may be associated with tumor metastasis in lung giant cells and hepatoma cancer cells, where elevated *GAL3ST2* expression is associated with higher metastatic potential (46). Previous studies have identified *GAL3ST2* expression in a normal murine mammary gland and in two human breast cancer cell lines, and elevated expression levels in metastatic tumors (47,48). *SAA* is an acute phase protein that may be the precursor of amyloid fibrils in reactive systemic amyloidosis (49) and function in cancer pathogenesis (50). *SAA1* may be a negative prognostic factor for patients with melanoma and further studies should assess these associations in other types of cancer (51). *SAA1* is overexpressed in plasma from patients with non-small cell lung cancer who experience short overall survival after treatment with epidermal growth factor receptor tyrosine-kinase inhibitors (52). *SBSN* is an epidermal differentiation marker that is detectable in several types of tumor endothelial cells (53,54). *SBSN* expression is associated with the growth, proliferation and invasiveness of salivary gland adenoid cystic and normal small cell lung carcinoma cells, as well as glioblastoma (55-58). *SOX2*, a transcription factor expressed in various types of embryonic and adult stem cells, is significantly upregulated in cancer stem cells of squamous skin tumors in mice (59). Furthermore, *SOX2* establishes a continuum between tumor initiation and progression in primary skin tumors (59), and its expression is required for the proliferation and anchorage-independent growth of lung and esophageal cell lines (60,61). *ZIC2* belongs to a gene family that was originally identified by homology with odd-paired genes in *Drosophila*, and functions during neural development (62). *ZIC2* has oncogenic features and its overexpression is closely associated with the progression of cervical, epithelial ovarian and liver cancer (63-65). Although the seven genes in the first group are all associated with human

tumors, their involvement in ccRCC is unknown. The second group contains only one gene, *WFDC13*. WAP domains are widely distributed and highly conserved in vertebrates and invertebrates, and they participate in diverse physiological processes, such as calcium transport, proteinase inhibition and bacterial killing (66). The WFDC proteins contain WAP domains and are found in vertebrates and invertebrates (66). *WFDC2* is frequently overexpressed in epithelial ovarian cancer cells and may have potential as a therapeutic target (67). However, the biological function of *WFDC13* in tumor progression remains unclear. The third group contains *IGLL1* and *PLG*, which have unknown functions.

The present findings suggested that the 10 DElncRNAs of the optimal combination may be involved in the pathogenesis of ccRCC. Among the 10 DElncRNAs, *COL18A1-AS1* (68,69), *TCL6* (70) and *TFAP2A-AS1* (71) are associated with a worse survival of patients with ccRCC, in accordance with the results of the present study. Furthermore, *ELOVL2-AS1*, *LINC00189*, *LINC00470*, *LINC00896* and *MIR205HG* may be associated with tumors other than ccRCC. For instance, *ELOVL2-AS1* may be a progression-associated prognostic biomarker for lung squamous cell carcinoma (72). *LINC00189* is associated with cervical cancer recurrence and may be used as a potential prognostic biomarker (73). Upregulated *LINC00470* expression promotes the development of gastric cancer (74). *LINC00896* expression is upregulated in human lung adenocarcinoma (75) and *MIR205HG* is differentially expressed in papillary renal cell carcinoma (76). However, few studies have investigated the functions of *LINC00652* and *UPK1A-AS1* in tumors. Despite considerable effort to determine the underlying mechanisms of lncRNAs in cancer, how they regulate gene expression remains elusive. Further studies are required to verify these prognostic DElncRNAs in ccRCC.

Functional annotations of the significant DEGs between the high- and low-risk groups of the entire set determined by the 10 DErnRNA expression risk scores according to the GO and KEGG databases may provide an ample number of candidate genes and further information regarding the pathogenesis of ccRCC. GO functional analyses of 400 DEGs were conducted, and 11 GO terms and 5 KEGG signaling pathways validated the significant enrichment of these DEGs. These genes were significantly associated with biological processes, such as 'inflammatory response', 'neuron differentiation' and 'acute inflammatory response', and participated in signaling pathways, such as 'complement and coagulation cascades' and 'neuroactive ligand-receptor interaction', suggesting potential functions for the 10 prognostic DErnRNAs in ccRCC. Further investigation of these genes may help to further clarify the pathogenesis of ccRCC. Since the present extensive bioinformatics study was based on published data, the results of the present study should be further validated *in vitro* and/or *in vivo*. Expression of these genes in ccRCC can be detected using reverse transcription PCR or the protein levels could be examined using western blotting.

In conclusion, the present study constructed risk score models based on the status or expression levels of 10 DElncRNAs or 10 DErnRNAs to predict the prognosis of patients with ccRCC, revealing that the prognostic performance of the model based on the expression levels of the 10 DErnRNAs was the

most effective. The 10 prognostic DEmRNAs were mainly associated with inflammatory response-associated biological processes, complement and coagulation cascades and neuroactive ligand-receptor interaction pathways. The 10 DEmRNAs in the optimal combination may be used as potential therapeutic targets, and the present results may provide novel insights into the pathogenesis of ccRCC.

Acknowledgements

Not applicable.

Funding

The present study was supported by National Natural Science Foundation of China (grant no. 81603441), Science and Technology Agency Foundation of Sichuan Province of China (grant no. 2017JY0297), Chengdu Medical College Foundation (grant no. CYZ15-11) and Health and Health Commission of Sichuan Province of China (grant no. 18ZD041).

Availability of data and materials

All datasets generated and/or analyzed during the current study are available in TCGA database (<https://gdc-portal.nci.nih.gov/>) or EBI Array database (dataset number, E-TABM-3267; <https://www.ebi.ac.uk/arrayexpress/>).

Authors' contributions

LY designed the present study. DX, WD, SW, BH and BG performed the data analysis. DX and WD drafted the manuscript. All authors read and approved the final manuscript.

Ethics approval and consent to participate

Not applicable.

Patient consent for publication

Not applicable.

Competing interests

The authors declare that they have no competing interests.

References

- Rini BI, Campbell SC and Escudier B: Renal cell carcinoma. *Lancet* 373: 1119-1132, 2009.
- Cancer Genome Atlas Research Network: Comprehensive molecular characterization of clear cell renal cell carcinoma. *Nature* 499: 43-49, 2013.
- Valera VA and Merino MJ: Misdiagnosis of clear cell renal cell carcinoma. *Nat Rev Urol* 8: 321-333, 2011.
- Aref S, Al Khodary T, Zeed TA, El Sadiq A, El Menshawy N and Al Ashery R: The prognostic relevance of BAALC and ERG expression levels in cytogenetically normal pediatric acute myeloid leukemia. *Indian J Hematol Blood Transfus* 31: 21-28, 2015.
- Li L, Feng T, Qu J, Feng N, Wang Y, Ma RN, Li X, Zheng ZJ, Yu H and Qian B: LncRNA expression signature in prediction of the prognosis of lung adenocarcinoma. *Genet Test Mol Biomarkers* 22: 20-28, 2018.
- Miller A, McLeod L, Alhanyani S, Szczepny A, Watkins DN, Chen W, Enriori P, Ferlin W, Ruwanpura S and Jenkins BJ: Blockade of the IL-6 trans-signalling/STAT3 axis suppresses cachexia in Kras-induced lung adenocarcinoma. *Oncogene* 36: 3059-3066, 2017.
- Tripathi MK, Doxtater K, Keramatnia F, Zacheaus C, Yallapu MM, Jaggi M and Chauhan SC: Role of lncRNAs in ovarian cancer: Defining new biomarkers for therapeutic purposes. *Drug Discov Today* 23: 1635-1643, 2018.
- Yao J, Chen Y, Wang Y, Liu S, Yuan X, Pan F and Geng P: Decreased expression of a novel lncRNA CADM1-AS1 is associated with poor prognosis in patients with clear cell renal cell carcinomas. *Int J Clin Exp Pathol* 7: 2758-2767, 2014.
- Hakimi AA, Reznik E, Lee C-H, Creighton CJ, Brannon AR, Luna A, Aksoy BA, Liu EM, Shen R, Lee W, *et al*: An integrated metabolic atlas of clear cell renal cell carcinoma. *Cancer Cell* 29: 104-116, 2016.
- Huang H, Ling W, Qiu T and Luo Y: Ultrasonographic features of testicular metastasis from renal clear cell carcinoma that mimics a seminoma: A case report. *Medicine (Baltimore)* 97: e12728, 2018.
- Chen J, Chen Y, Gu L, Li X, Gao Y, Lyu X, Chen L, Luo G, Wang L, Xie Y, *et al*: LncRNAs act as prognostic and diagnostic biomarkers in renal cell carcinoma: A systematic review and meta-analysis. *Oncotarget* 7: 74325-74336, 2016.
- Deng M, Blondeau JJ, Schmidt D, Perner S, Müller SC and Ellinger J: Identification of novel differentially expressed lncRNA and mRNA transcripts in clear cell renal cell carcinoma by expression profiling. *Genom Data* 5: 173-175, 2015.
- Ning L, Li Z, Wei D, Chen H and Yang C: LncRNA, NEAT1 is a prognosis biomarker and regulates cancer progression via epithelial-mesenchymal transition in clear cell renal cell carcinoma. *Cancer Biomark* 19: 75-83, 2017.
- Chen J-M, Cooper DN, Chuzhanova N, Férec C and Patrino GP: Gene conversion: Mechanisms, evolution and human disease. *Nat Rev Genet* 8: 762-775, 2007.
- Iida M, Ikeda F, Hata J, Hirakawa Y, Ohara T, Mukai N, Yoshida D, Yonemoto K, Esaki M, Kitazono T, *et al*: Development and validation of a risk assessment tool for gastric cancer in a general Japanese population. *Gastric Cancer* 21: 383-390, 2018.
- Hung YC, Lin CL, Liu CJ, Hung H, Lin SM, Lee SD, Chen PJ, Chuang SC and Yu MW: Development of risk scoring system for stratifying population for hepatocellular carcinoma screening. *Hepatology* 61: 1934-1944, 2015.
- Hussein AA, Ghani KR, Peabody J, Sarle R, Abaza R, Eun D, Hu J, Fumo M, Lane B, Montgomery JS, *et al*: Michigan Urological Surgery Improvement Collaborative and Applied Technology Laboratory for Advanced Surgery Program: Development and validation of an objective scoring tool for robot-assisted radical prostatectomy: Prostatectomy assessment and competency evaluation. *J Urol* 197: 1237-1244, 2017.
- Klatte T, Seligson DB, LaRochelle J, Shuch B, Said JW, Riggs SB, Zomorodian N, Kabbavar FF, Pantuck AJ and Beldegrun AS: Molecular signatures of localized clear cell renal cell carcinoma to predict disease-free survival after nephrectomy. *Cancer Epidemiol Biomarkers Prev* 18: 894-900, 2009.
- Heinzelmann J, Henning B, Sanjmyatav J, Posorski N, Steiner T, Wunderlich H, Gajda MR and Junker K: Specific miRNA signatures are associated with metastasis and poor prognosis in clear cell renal cell carcinoma. *World J Urol* 29: 367-373, 2011.
- Takahashi M, Rhodes DR, Furge KA, Kanayama H, Kagawa S, Haab BB and Teh BT: Gene expression profiling of clear cell renal cell carcinoma: Gene identification and prognostic classification. *Proc Natl Acad Sci USA* 98: 9754-9759, 2001.
- Wu X, Weng L, Li X, Guo C, Pal SK, Jin JM, Li Y, Nelson RA, Mu B, Onami SH, *et al*: Identification of a 4-microRNA signature for clear cell renal cell carcinoma metastasis and prognosis. *PLoS One* 7: e35661, 2012.
- Beuselinck B, Job S, Becht E, Karadimou A, Verkarre V, Couchy G, Giraldo N, Rioux-Leclercq N, Molinié V, Sibony M, *et al*: Molecular subtypes of clear cell renal cell carcinoma are associated with sunitinib response in the metastatic setting. *Clin Cancer Res* 21: 1329-1339, 2015.
- Parkinson H, Kapushesky M, Kolesnikov N, Rustici G, Shojatalab M, Abeygunawardena N, Berube H, Dylag M, Emam I, Farne A, *et al*: ArrayExpress update--from an archive of functional genomics experiments to the atlas of gene expression. *Nucleic Acids Res* 37 (Database): D868-D872, 2009.

24. Wright MW: A short guide to long non-coding RNA gene nomenclature. *Hum Genomics* 8: 7, 2014.
25. Ritchie ME, Phipson B, Wu D, Hu Y, Law CW, Shi W and Smyth GK: limma powers differential expression analyses for RNA-sequencing and microarray studies. *Nucleic Acids Res* 43: e47, 2015.
26. R Development Core Team R: A language and environment for statistical computing. R Foundation for Statistical Computing, Vienna, 2011. <http://www.R-project.org>
27. Ito K and Murphy D: Application of ggplot2 to Pharmacometric Graphics. *CPT Pharmacometrics Syst Pharmacol* 2: e79, 2013.
28. Wang L, Cao C, Ma Q, Zeng Q, Wang H, Cheng Z, Zhu G, Qi J, Ma H, Nian H, *et al*: RNA-seq analyses of multiple meristems of soybean: Novel and alternative transcripts, evolutionary and functional implications. *BMC Plant Biol* 14: 169, 2014.
29. Wang P, Wang Y, Hang B, Zou X and Mao JH: A novel gene expression-based prognostic scoring system to predict survival in gastric cancer. *Oncotarget* 7: 55343-55351, 2016.
30. Tibshirani R: The lasso method for variable selection in the Cox model. *Stat Med* 16: 385-395, 1997.
31. Goeman JJ: L1 penalized estimation in the Cox proportional hazards model. *Biom J* 52: 70-84, 2010.
32. Camp RL, Dolled-Filhart M and Rimm DL: X-tile: A new bio-informatics tool for biomarker assessment and outcome-based cut-point optimization. *Clin Cancer Res* 10: 7252-7259, 2004.
33. Gettman MT, Blute ML, Spotts B, Bryant SC and Zincke H: Pathologic staging of renal cell carcinoma: Significance of tumor classification with the 1997 TNM staging system. *Cancer* 91: 354-361, 2001.
34. Delahunt B, Eble JN, Egevad L and Samaratunga H: Grading of renal cell carcinoma. *Histopathology* 74: 4-17, 2019.
35. Anderson WI, Schlafer DH and Vesely KR: Thyroid follicular carcinoma with pulmonary metastases in a beaver (*Castor canadensis*). *J Wildl Dis* 25: 599-600, 1989.
36. Eng KH, Schiller E and Morrell K: On representing the prognostic value of continuous gene expression biomarkers with the restricted mean survival curve. *Oncotarget* 6: 36308-36318, 2015.
37. Iasonos A, Schrag D, Raj GV and Panageas KS: How to build and interpret a nomogram for cancer prognosis. *J Clin Oncol* 26: 1364-1370, 2008.
38. Huang G, Zhao G, Xia J, Wei Y, Chen F, Chen J and Shi J: FGF2 and FAM201A affect the development of osteonecrosis of the femoral head after femoral neck fracture. *Gene* 652: 39-47, 2018.
39. Klatte T and Rossi SH: Prognostic factors and prognostic models for renal cell carcinoma: a literature review. *World J Urol* 36: 1943-1952, 2018.
40. Adam PJ, Boyd R, Tyson KL, Fletcher GC, Stamps A, Hudson L, Poyser HR, Redpath N, Griffiths M, Steers G, *et al*: Comprehensive proteomic analysis of breast cancer cell membranes reveals unique proteins with potential roles in clinical cancer. *J Biol Chem* 278: 6482-6489, 2003.
41. King ER, Tung CS, Tsang YTM, Zu Z, Lok GT, Deavers MT, Malpica A, Wolf JK, Lu KH, Birrer MJ, *et al*: The anterior gradient homolog 3 (AGR3) gene is associated with differentiation and survival in ovarian cancer. *Am J Surg Pathol* 35: 904-912, 2011.
42. Obacz J, Takacova M, Brychtova V, Dobes P, Pastorekova S, Vojtesek B and Hrstka R: The role of AGR2 and AGR3 in cancer: Similar but not identical. *Eur J Cell Biol* 94: 139-147, 2015.
43. Qiu C, Wang Y, Wang X, Zhang Q, Li Y, Xu Y, Jin C, Bu H, Zheng W, Yang X, *et al*: Combination of TP53 and AGR3 to distinguish ovarian high-grade serous carcinoma from low-grade serous carcinoma. *Int J Oncol* 52: 2041-2050, 2018.
44. He J-Q, Shumansky K, Connett JE, Anthonisen NR, Paré PD and Sandford AJ: Association of genetic variations in the CSF2 and CSF3 genes with lung function in smoking-induced COPD. *Eur Respir J* 32: 25-34, 2008.
45. Lee Y-Y, Wu W-J, Huang C-N, Li CC, Li WM, Yeh BW, Liang PI, Wu TF and Li CF: CSF2 overexpression is associated with STAT5 phosphorylation and poor prognosis in patients with urothelial carcinoma. *J Cancer* 7: 711-721, 2016.
46. Shi B-Z, Hu P, Geng F, He P-J and Wu X-Z: Gal3ST-2 involved in tumor metastasis process by regulation of adhesion ability to selectins and expression of integrins. *Biochem Biophys Res Commun* 332: 934-940, 2005.
47. Guerra LN, Suárez C, Soto D, Schiappacasse A, Sapochnik D, Sacca P, Piwien-Pilipuk G, Peral B and Calvo JC: GAL3ST2 from mammary gland epithelial cells affects differentiation of 3T3-L1 preadipocytes. *Clin Transl Oncol* 17: 511-520, 2015.
48. Qin F, Song Z, Chang M, Song Y, Frierson H and Li H: Recurrent cis-SAGE chimeric RNA, D2HGDH-GAL3ST2, in prostate cancer. *Cancer Lett* 380: 39-46, 2016.
49. Turnell W, Sarra R, Glover ID, Baum JO, Caspi D, Baltz ML and Pepys MB: Secondary structure prediction of human SAA1. Presumptive identification of calcium and lipid binding sites. *Mol Biol Med* 3: 387-407, 1986.
50. Sung H-J, Ahn J-M, Yoon Y-H, Rhim TY, Park CS, Park JY, Lee SY, Kim JW and Cho JY: Identification and validation of SAA as a potential lung cancer biomarker and its involvement in metastatic pathogenesis of lung cancer. *J Proteome Res* 10: 1383-1395, 2011.
51. Mattarollo SR and Smyth MJ: A novel axis of innate immunity in cancer. *Nat Immunol* 11: 981-982, 2010.
52. Milan E, Lazzari C, Anand S, Floriani I, Torri V, Sorlini C, Gregorc V and Bachi A: SAA1 is over-expressed in plasma of non small cell lung cancer patients with poor outcome after treatment with epidermal growth factor receptor tyrosine-kinase inhibitors. *J Proteomics* 76: 91-101, 2012.
53. Alam MT, Nagao-Kitamoto H, Ohga N, Akiyama K, Maishi N, Kawamoto T, Shinohara N, Taketomi A, Shindoh M, Hida Y, *et al*: Suprabasin as a novel tumor endothelial cell marker. *Cancer Sci* 105: 1533-1540, 2014.
54. Park GT, Lim SE, Jang S-I and Morasso MI: Suprabasin, a novel epidermal differentiation marker and potential cornified envelope precursor. *J Biol Chem* 277: 45195-45202, 2002.
55. Formolo CA, Williams R, Gordish-Dressman H, MacDonald TJ, Lee NH and Hathout Y: Secretome signature of invasive glioblastoma multiforme. *J Proteome Res* 10: 3149-3159, 2011.
56. Glazer CA, Smith IM, Ochs MF, Begum S, Westra W, Chang SS, Sun W, Bhan S, Khan Z, Ahrendt S, *et al*: Integrative discovery of epigenetically depressed cancer testis antigens in NSCLC. *PLoS One* 4: e8189, 2009.
57. Shao C, Tan M, Bishop JA, Liu J, Bai W, Gaykalova DA, Ogawa T, Vikani AR, Agrawal Y, Li RJ, *et al*: Suprabasin is hypomethylated and associated with metastasis in salivary adenoid cystic carcinoma. *PLoS One* 7: e48582, 2012.
58. Zhu J, Wu G, Li Q, Gong H, Song J, Cao L, Wu S, Song L and Jiang L: Overexpression of suprabasin is associated with proliferation and tumorigenicity of esophageal squamous cell carcinoma. *Sci Rep* 6: 21549, 2016.
59. Boumahdi S, Driessens G, Lapouge G, Rorive S, Nassar D, Le Mercier M, Delatte B, Caauwe A, Lenglez S, Nkusi E, *et al*: SOX2 controls tumour initiation and cancer stem-cell functions in squamous-cell carcinoma. *Nature* 511: 246-250, 2014.
60. Bass AJ, Watanabe H, Mermel CH, Yu S, Perner S, Verhaak RG, Kim SY, Wardwell L, Tamayo P, Gat-Viks I, *et al*: SOX2 is an amplified lineage-survival oncogene in lung and esophageal squamous cell carcinomas. *Nat Genet* 41: 1238-1242, 2009.
61. Leis O, Eguiara A, Lopez-Arribillaga E, Alberdi MJ, Hernandez-Garcia S, Elorriaga K, Pandiella A, Rezola R and Martin AG: Sox2 expression in breast tumours and activation in breast cancer stem cells. *Oncogene* 31: 1354-1365, 2012.
62. Elms P, Siggers P, Napper D, Greenfield A and Arkell R: Zic2 is required for neural crest formation and hindbrain patterning during mouse development. *Dev Biol* 264: 391-406, 2003.
63. Chan DW, Liu VW, Leung LY, Yao KM, Chan KK, Cheung AN and Ngan HY: Zic2 synergistically enhances Hedgehog signalling through nuclear retention of Gli1 in cervical cancer cells. *J Pathol* 225: 525-534, 2011.
64. Marchini S, Poynor E, Barakat RR, Clivio L, Cinquini M, Fruscio R, Porcu L, Bussani C, D'Incalci M, Erba E, *et al*: The zinc finger gene ZIC2 has features of an oncogene and its overexpression correlates strongly with the clinical course of epithelial ovarian cancer. *Clin Cancer Res* 18: 4313-4324, 2012.
65. Zhu P, Wang Y, He L, Huang G, Du Y, Zhang G, Yan X, Xia P, Ye B, Wang S, *et al*: ZIC2-dependent OCT4 activation drives self-renewal of human liver cancer stem cells. *J Clin Invest* 125: 3795-3808, 2015.
66. Smith VJ: Phylogeny of whey acidic protein (WAP) four-disulfide core proteins and their role in lower vertebrates and invertebrates. *Biochem Soc Trans* 39: 1403-1408, 2011.
67. Chen Y, Mu X, Wang S, Zhao L, Wu Y, Li J and Li M: WAP four-disulfide core domain protein 2 mediates the proliferation of human ovarian cancer cells through the regulation of growth- and apoptosis-associated genes. *Oncol Rep* 29: 288-296, 2013.
68. Wang J, Zhang C, He W and Gou X: Construction and comprehensive analysis of dysregulated long non-coding RNA-associated competing endogenous RNA network in clear cell renal cell carcinoma. *J Cell Biochem* 120: 2576-2593, 2018.

69. Liu T, Sui J, Zhang Y, Zhang XM, Wu WJ, Yang S, Xu SY, Hong WW, Peng H, Yin LH, *et al*: Comprehensive analysis of a novel lncRNA profile reveals potential prognostic biomarkers in clear cell renal cell carcinoma. *Oncol Rep* 40: 1503-1514, 2018.
70. Su H, Sun T, Wang H, Shi G, Zhang H, Sun F and Ye D: Decreased TCL6 expression is associated with poor prognosis in patients with clear cell renal cell carcinoma. *Oncotarget* 8: 5789-5799, 2017.
71. Jiang W, Guo Q, Wang C and Zhu Y: A nomogram based on 9-lncRNAs signature for improving prognostic prediction of clear cell renal cell carcinoma. *Cancer Cell Int* 19: 208-208, 2019.
72. Wang Y, Yang F and Zhuang Y: Identification of a progression-associated long non-coding RNA signature for predicting the prognosis of lung squamous cell carcinoma. *Exp Ther Med* 15: 1185-1192, 2018.
73. Zhang Y, Zhang X, Zhu H, Liu Y, Cao J, Li D, Ding B, Yan W, Jin H and Wang S: Identification of Potential prognostic long non-coding RNA biomarkers for predicting recurrence in patients with cervical cancer. *Cancer Manag Res* 12: 719-730, 2020.
74. Yan J, Huang X, Zhang X, Chen Z, Ye C, Xiang W and Huang Z: LncRNA LINC00470 promotes the degradation of PTEN mRNA to facilitate malignant behavior in gastric cancer cells. *Biochem Biophys Res Commun* 521: 887-893, 2020.
75. Sui J, Li YH, Zhang YQ, Li CY, Shen X, Yao WZ, Peng H, Hong WW, Yin LH, Pu YP, *et al*: Integrated analysis of long non-coding RNA-associated ceRNA network reveals potential lncRNA biomarkers in human lung adenocarcinoma. *Int J Oncol* 49: 2023-2036, 2016.
76. Luo Q, Cui M, Deng Q and Liu J: Comprehensive analysis of differentially expressed profiles and reconstruction of a competing endogenous RNA network in papillary renal cell carcinoma. *Mol Med Rep* 19: 4685-4696, 2019.



This work is licensed under a Creative Commons Attribution-NonCommercial-NoDerivatives 4.0 International (CC BY-NC-ND 4.0) License.